Supporting Information

Understanding the Formation Mechanism of Magnetic Mesocrystals with (Cryo-) Electron Microscopy

Giulia Mirabello, Arthur Keizer, Paul H. H. Bomans, András Kovács, Rafal E. Dunin-Borkowski, Nico A.J.M. Sommerdijk and Heiner Friedrich**

Corresponding Author

* E-mail: h.friedrich@tue.nl (H.F.). * E-mail: n.sommerdijk@tue.nl (N.A.J.M.S.).

1. Additional cryo-TEM images

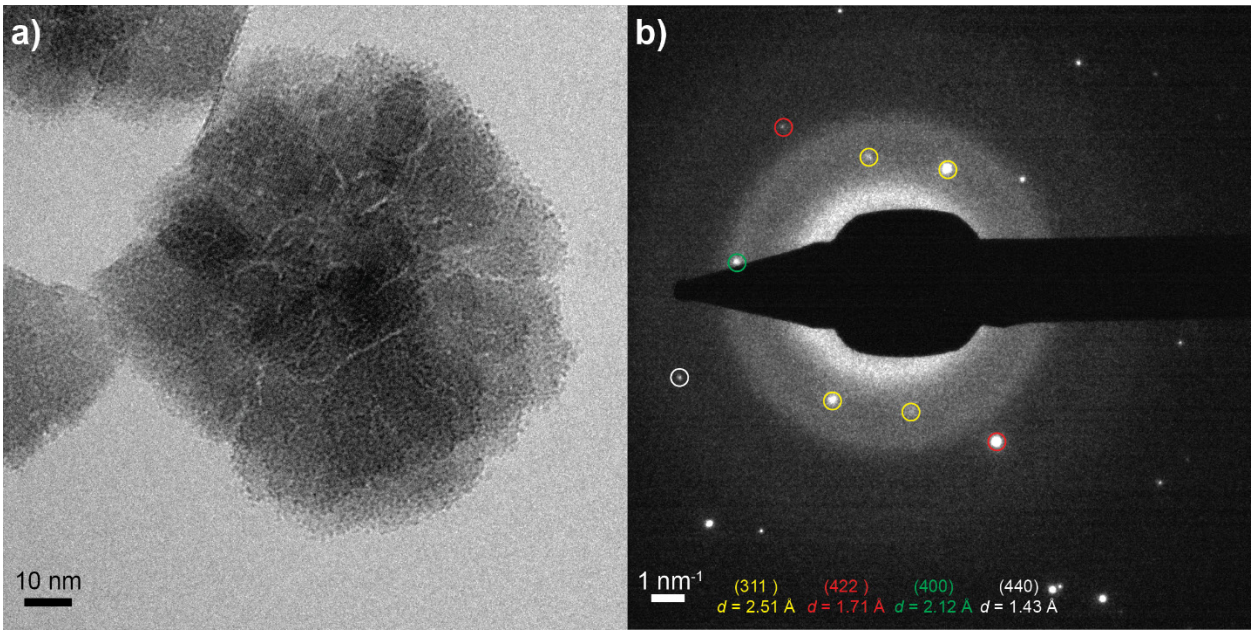

Figure S1. a) Cryo-TEM image and b) selected area electron diffraction pattern of a typical flower-like magnetite aggregate. Insets in b) show the reflection indexing of the most common crystalline plane for magnetite.[1]

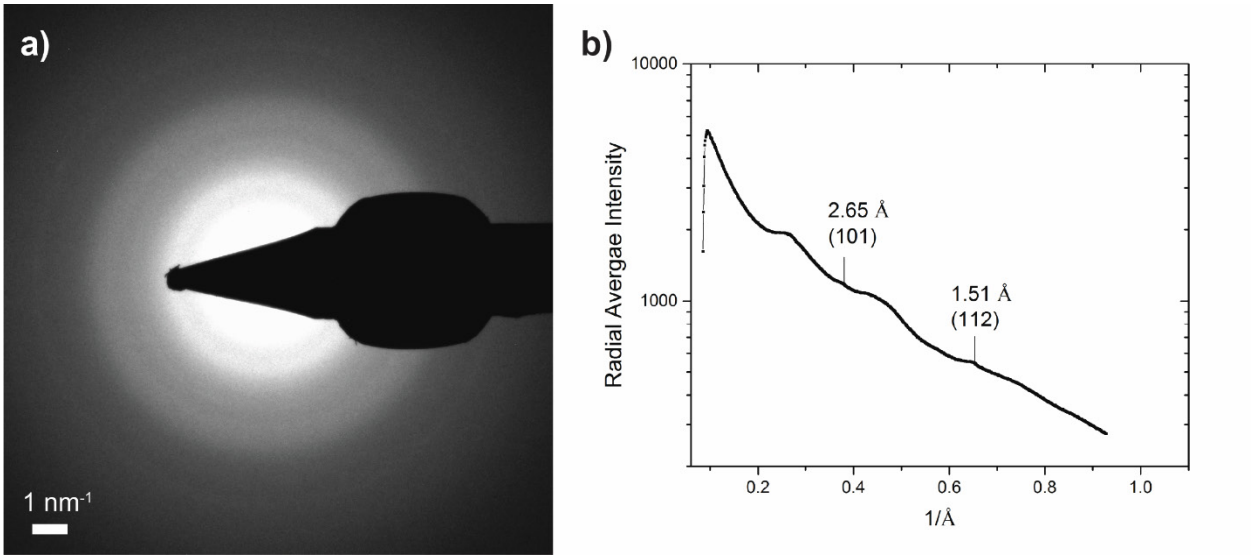

Figure S2. Analysis of the selected area electron diffraction pattern of star-like green rust aggregates. a) Brightness and contrast adjusted pattern to increase visibility of the diffraction ring. b) Radial average profile showing two weak reflection consistent with green rust. [2] The original electron diffraction pattern is shown in Figure 1d.

Figure S.3 and S.4 shows the cryo-TEM micrographs of the solution during the reaction at different times. In Figure S3a two isolated Fe_3O_4 aggregates are shown, where green rust platelets seem to interact closely with the structure. Figure S3b shows magnetite subunits in proximity of a string of Fe_3O_4 aggregates, supporting the hypothesis of an aggregation mechanism for the formation of the nanoflower magnetite crystals. In Figure S3c green rust platelets can be seen, where the ideal hexagonal shape is lost due to the dissolution process, also fracture is visible at the edge. In Figure S3d isolated magnetite crystals are observed together with the green rust. The green rust is significantly reduced in size and appears to be more dispersed as compared with previous time points. Figure S4 shows the cryo-TEM micrographs and the corresponding SAED patterns of isolated Fe_3O_4 aggregates at early stages during the reaction. The SAED pattern, illustrated in Figure S4b and d, show a single-crystal-like electron diffraction pattern. The reflections which are not in the single-crystal-like pattern may originate from subunits that are not aligned or by green rust crystals present in the background of the acquisition area, highlighted with a yellow circle in Figure S4a and c.

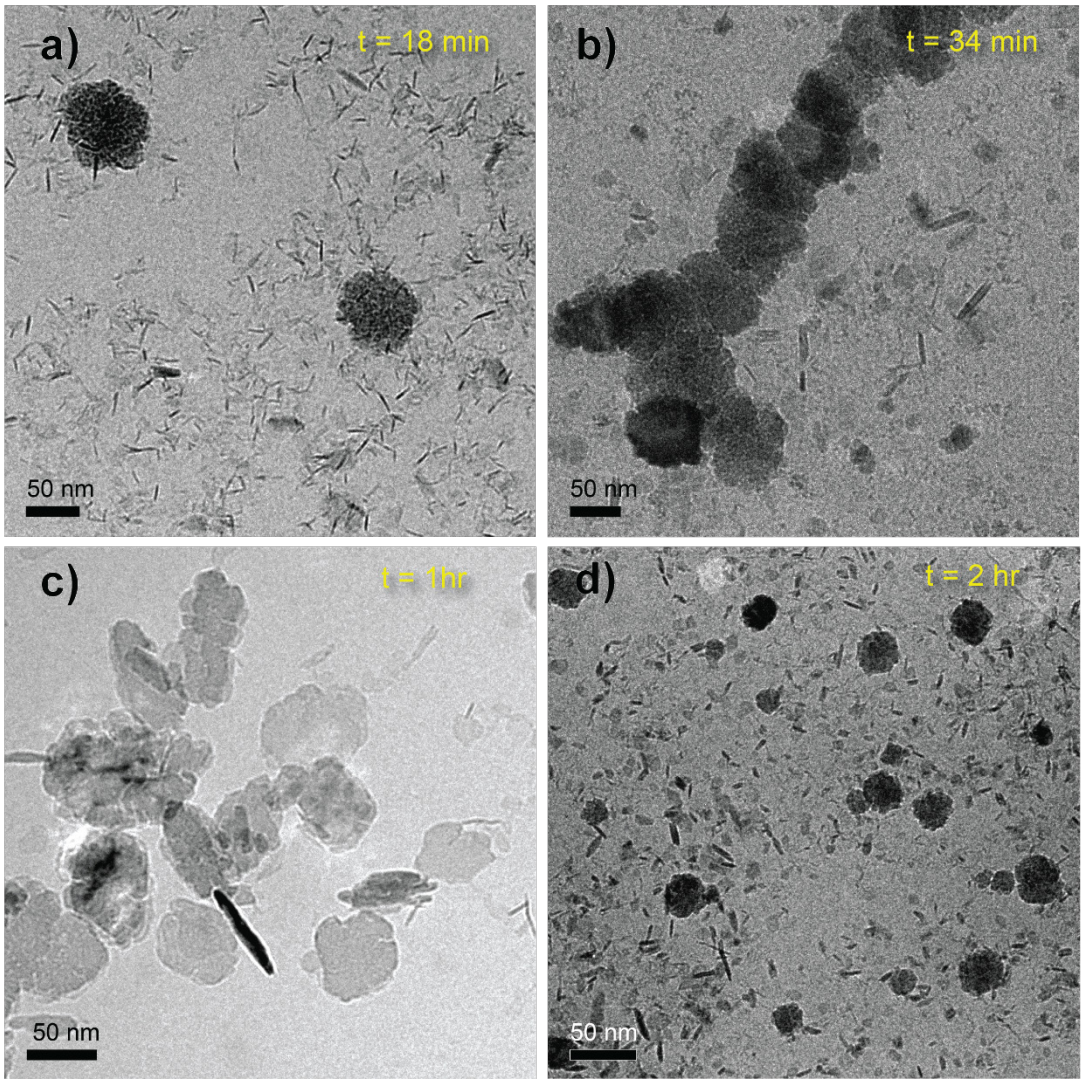

Figure S3. Cryo-TEM micrographs of samples during the reaction: a) 18 min, b) 34 min, c) 1 hour and d) 2 hours.

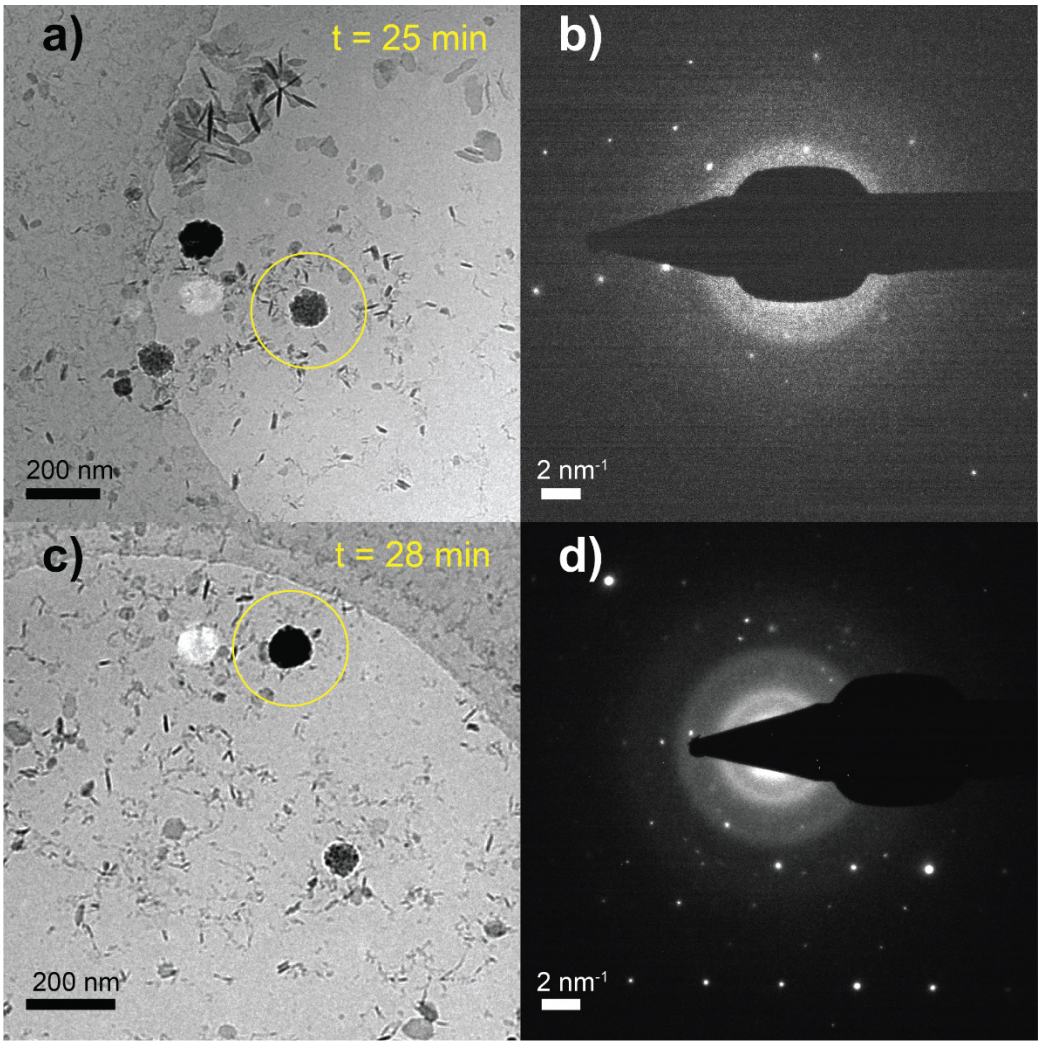

Figure S4. a, c) Cryo-TEM micrographs and b, c) SAED pattern of isolated Fe_3O_4 aggregates at a, b) 25 min and c, d) 28 min reaction time.

2. Green rust

Green rust is a mixed valence iron (Fe^{2+} - Fe^{3+}) hydroxide with green/bluish color, formed by the oxidation of Fe^{2+} at alkaline pH with a variable Fe^{2+} : Fe^{3+} ratio,[3] constituted of hexagonal thin platelets. Green rust is isostructural to pyroaurite ($Mg_6Fe_2(OH)_{16}CO_3$), consisting of sheets in which some of the Fe^{2+} is replaced by Fe^{3+}.[4] The presence of Fe^{3+} generates a positive charge that is balanced by the incorporation of anions between the sheets. Green rust is classified either as "type 1" or "type 2" depending on the counter anions, Cl^- for type 1 and SO_4^{2-} for type 2. The green rust obtained in this work is type 2 given that only SO_4^{2-} ions are available as the counter ion in solution.

3. Colloidal stability: pAA adsorption effects

Polymer adsorption is energetically favorable when the loss of configurational entropy caused by the interaction between the colloid surface and the polymer segments is compensated [5]. The adsorbed polymer can produce two different effects depending degree of adsorption (Γ). When the surfaces of the particles are completely saturated with the adsorbed polymer, the dispersion will be kinetically stabilized. This effect is caused by the dense polymer layers around the particles that gives rise to a steric repulsive interaction. On the contrary, when the surface of the particles are not saturated, the thin polymer layer cannot inhibit the approaching of the particles. Moreover, the polymer chains can interact with the surface of other particles forming the so-called *bridges*, promoting the attraction between particles. The phenomena is known as *bridging flocculation* [5] and it is accentuated when the polymer is a polyelectrolyte and/or has high molecular weight (M_w). Typically the polymer adsorbed amount at saturation is $\Gamma \sim 1$ mg $\cdot$ m^{-2}.[5]

A completely different effect is caused by the presence of a nonadsorbing polymer in solution. The fact that the polymer does not adsorb on the surface particles induces an interaction between the colloids. This interaction is the result of the overlap of the *depletion layers*, located around the particles, which in turns minimizes the free energy of the polymer. As a consequence, states where the particles are close together are more favorable and the polymer indirectly induces the attractive interactions between particles. [6-8]

In our experiments we used polyacrylic acid, pAA, with $M_w \sim 450$ kDa that is a negatively charged at alkaline pH. The formation of the green rust star-like aggregate, observed in the early stages of magnetite formation by cryo-TEM (see Figure1d), could be due to the bridging flocculation. In our experimental conditions Γ has an estimated value ~ 1 mg $\cdot$ m^{-2}, suggesting that indeed the flocculation is possible. While magnetite is formed, the green rust is consumed with, consequently, a reduction of their surface, as observed in cryo-TEM, where their shape changes from the ideal hexagon (inset in Figure 5.1h and section 1 Figure S2c). As a consequence the platelet surface decreasing and the polymer stabilizes the green rust with consequence stop of the flocculation. In fact, as the reaction proceeds the star-like aggregates decreased in frequency. Nevertheless, star-like aggregates of green rust are observed up to 45 minutes reaction time. On the contrary, the open network formed by precursor platelets is observed up to two hours reaction time, however, their size is significantly decreased (see section 1 Figure S2d)

4. Time crystal size measurement

We measured the average crystal size of the magnetite aggregates as a function of the reaction time. The results of this analysis show that crystal size is approximately constant regardless the reaction time. However, a slightly increase in crystal size from 7 to 25 minutes of reaction is observed (Figure S3a). Further, we labelled the magnetite aggregate in terms of their aggregation type and compared their crystal size (Figure S3b). The magnetite crystals are divided in two categories: crystals arranged in string or stabilized in solution isolated crystals. The "string crystals" are further labeled in terms of the number of crystals contacts: 1) 1 contact represent the crystals at the end of the string; 2) 2 contacts represent the crystals that compose the segments of the string; 3) 3 or more contacts represent the crystals at the cross point of the multiple strings. Also, aggregates crystals arranged in pairs were found and labeled. The results of the labeling analysis shows that the average size is constant regardless the type of crystals (strings or isolated in solution), regardless the reaction time, suggesting that the polymer controls the growth process.

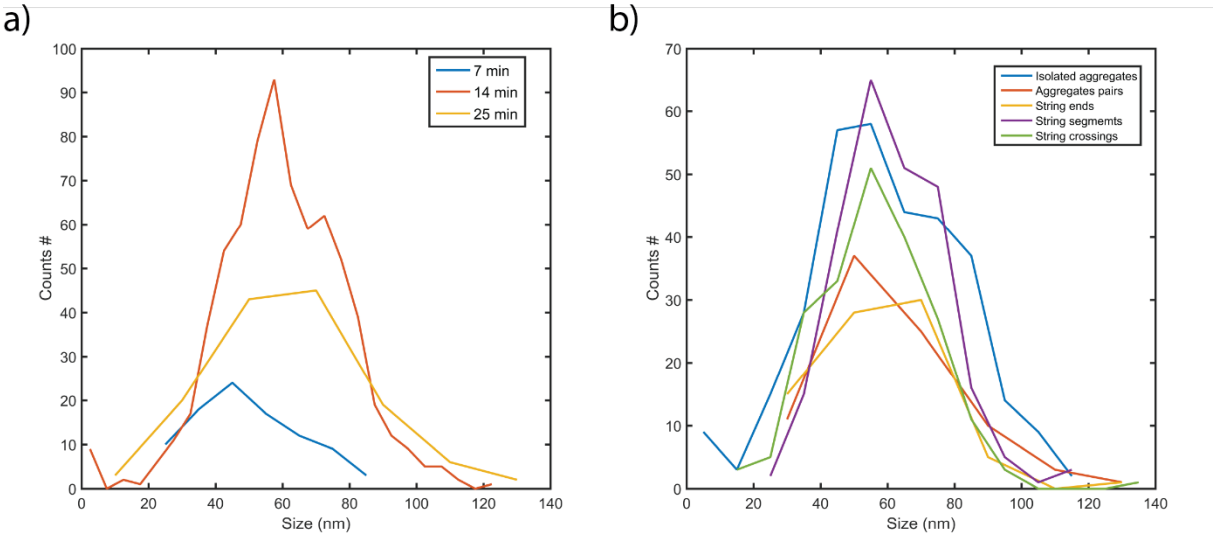

Figure S5. Measured average crystal size of the magnetite aggregates a) in terms of the reaction time and b) in terms of the crystal labeling from the sample vitrified at 14 min.

5. High-resolution electron tomography

5.1. Artifacts and resolution limit

In the reconstructed tomogram the *y*-axis is parallel to the rotation stage axis, thus the *x*-axis, perpendicular to *y*, is parallel to the 0° image plane, and the *z*-axis is perpendicular to both *x* and

y. Due to the acquisition conditions the resolution in the tomogram is anisotropic, as the *x*-direction is compressed because the tilting stage and the *z*-direction is extrapolated from *x* and *y* during the reconstruction. As a consequence, highest resolution can be achieved in the *y*-direction, while the lowest is the *z*-direction.

A low pass filter was applied to the tomographic tilt-series before the reconstruction to filter out the high frequency signals. The non-uniformity of the background as well as some horizontal striping visible in the reconstructed tomogram are due to the acquisition method used and to the reconstruction process and have to be considered as artifacts.

The tomographic tilted series was acquired at a magnification of 105 k (pixel size 0.095×0.095 nm) with a defocus value of –300 nm. The contrast transfer function is commonly used to determine the point resolution and the information limit of a TEM micrograph. The CTF describes the electron phase information transfer into the intensity image through self-interference. With our experimental acquisition condition we have estimated a point resolution of ~ 0.8 nm and an information limit of ~ 1.5 Å, allowing to get lattice information in each image of the tomographic tilt-series. The point resolution represents the minimum distance at which two objects can be distinguished as separate objects.

5.2. 3-D volume reconstructed visualization

The tomographic tilt-series is used to obtain the tomographic reconstruction, where the 2-D images acquired at different tilt angles are converted into a 3D image giving access to the volume organization of the crystals investigated. Alignment and reconstruction of the tilt-series were performed using IMOD. The segmentation and the 3-D volume visualization of the reconstructed tomogram were performed with the 3-D analysis Software package Avizo 8.1.

5.3. Volume segmentation of the subunits in Fe_3O_4 aggregate

The reconstructed tomogram of a single aggregate was processed with a multi-step algorithm in order to obtain the volume segmentation of the subunits composing the magnetite aggregate. The segmentation algorithm consists of 5 Matlab scripts and 2 manual segmentation steps. The first step has the purpose to enhance the signal of the gaps by denosing the images. This step is carried out by applying a one dimensional maximum filter with a length of 9 pixels (0.86 nm) in all 3 directions whose average gives the *filtered volume*. In the next step the aggregate and the gaps are

manually segmented in two separate moments, from the volume background with Avizo Software (Figure S6a). The obtained filtered volume, *aggregate segmentation* and *gaps segmentation* were processed with a distance-based watershed to obtain the distance transform map (Figure S6b) and thereafter the final volume labeling of the subunits (Figure 2b) was done. The final labelled segmentation volume was used to calculate the size range of the subunits by counting the pixel numbers (voxels) in the volume of each segmented subunits.

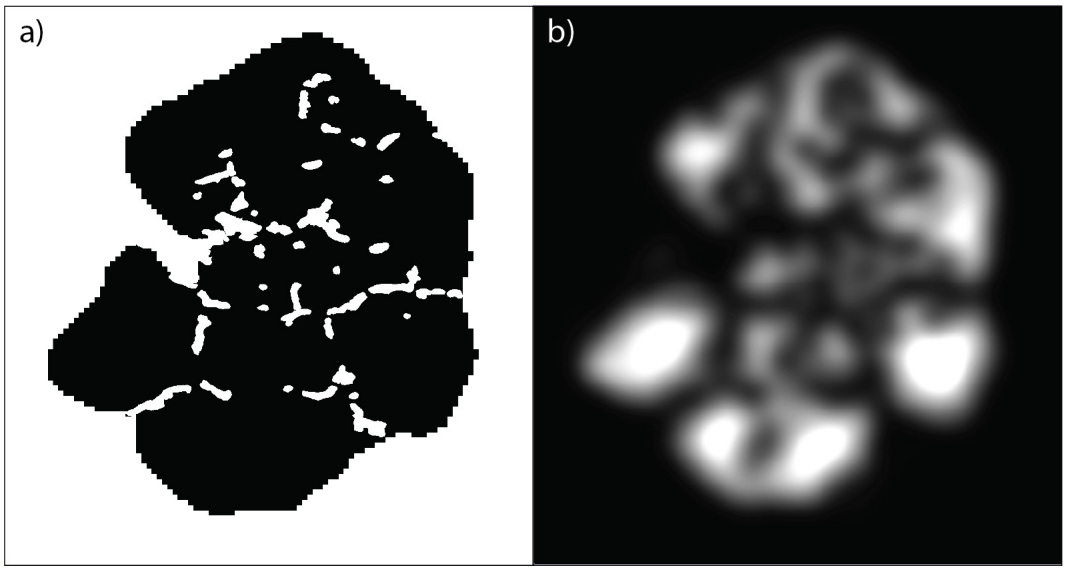

Figure S6. Representative slice of the subunits volume segmentation of the magnetite aggregate. a) Result of the manual segmentation of the aggregate and gaps. b) Distance transform map.

5.4. Crystallographic alignment

Each image acquired from the tomographic tilted series contains information on the crystal lattice represented by the striping pattern visible in the images (Figure 3). The fast Fourier transform (FFT) images in Figure 3b shows diffraction spots whose distance from the center corresponds to the *d*-spacing of a certain crystalline plane. The FFT series was further processed by Fourier filtering in order to enhance the area in the TEM image that produces a certain diffraction spot. Thus, this processing can help in visualizing the crystallographic alignment along a certain crystalline plane of the magnetite subunits of the aggregate. Figure 3 shows a representative example of the process above described.

6. Acquisition and analysis of the electron hologram

In the transmission electron microscope, an electrostatic biprism is employed to interfere the reference electron wave and the object electron wave that have passed through the vacuum and the specimen respectively. The interference of these two tilted wave components results in a fringe pattern or hologram where bending of the fringe records the phase of the electron wave and intensity modulations along the fringe records the amplitude of the electron wave For the acquisition of the hologram a positively charged biprism was used at 120 V voltage that results in ~ 2.6 nm fringe spacing. For the magnetization reversal experiment the sample stage was tilted to +75º and –75°, and magnetized using the full excitation of the objective lens applying an in-plane magnetic field of ~ 1.4 T to the sample. The objective lens was then switched off, the sample stage tilted back to 0° and the holograms were recorded at remanent state. The holograms were acquired in pairs where the sample was magnetically saturated in opposite directions, assuming that the magnetization state of the material is completely reversible. We investigate chains composed of several magnetite aggregate. Magnetite magnetization, M_0, is 0.6 T therefore we assume that the magnetic field within the chain is aligned in-plane to the saturating magnetic field. The applied magnetic field (H) direction is approximately the same as the main axis direction of the investigated magnetite chains. It should be noted, however, that no magnetic field is applied during the acquisition, but only before in the magnetization step. Assuming no significant charging of the sample is present during the electron holography experiment, the mean inner potential (MIP, ϕ_{MIP}) and the magnetic phase shift (ϕ_M) can be calculated from the acquired pairs of holograms. Figure S7a shows the magnetic phase shift map of Fe_3O_4 mesocrystal chain shown in Figure 4. An intensity linescan along A-A' is taken from a 70-nm-mesocrystal and plotted in Figure S7b showing the 1.5 rad step in the phase.

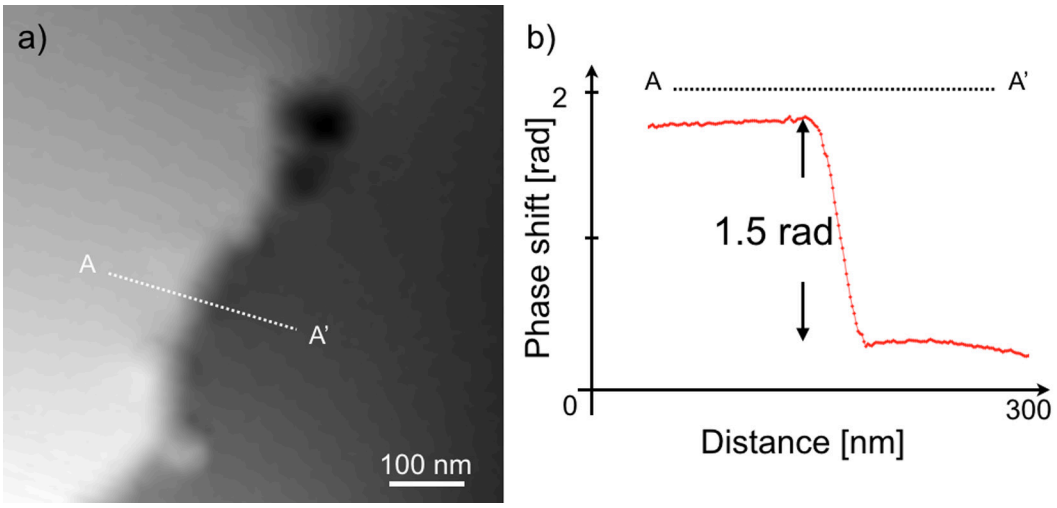

Figure S7. a) Magnetic phase (ϕ_M) map of Fe_3O_4 mesocrystal chain measured using off-axis electron holography. An intensity linescan is recorded along the A-A' and plotted in b).

References

(1) Cornell, R. M.; Schwertmann, U., *The iron oxides: structure, properties, reactions, occurrences and uses*. John Wiley & Sons: 2006.

(2) Altan, C. L.; Lenders, J. J. M.; Bomans, P. H. H.; de With, G.; Friedrich, H.; Bucak, S.; Sommerdijk, N. A. J. M., Partial Oxidation as a Rational Approach to Kinetic Control in Bioinspired Magnetite Synthesis. *Chemistry – A European Journal* **2015,** *21* (16), 6150-6156.

(3) Cornell, R. M.; Schwertmann, U., Crystal Structure. In *The Iron Oxides*, 2004.

(4) Trolard, F.; Bourrié, G., Structure of fougerite and green rusts and a thermodynamic model for their stabilities. *Journal of Geochemical Exploration* **2006,** *88* (1), 249-251.

(5) Fleer, G.; Stuart, M. C.; Scheutjens, J.; Cosgrove, T.; Vincent, B., *Polymers at interfaces*. Springer Science & Business Media: 1993.

(6) Asakura, S.; Oosawa, F., On Interaction between Two Bodies Immersed in a Solution of Macromolecules. *The Journal of Chemical Physics* **1954,** *22* (7), 1255-1256.

(7) Anderson, V. J.; Lekkerkerker, H. N. W., Insights into phase transition kinetics from colloid science. *Nature* **2002,** *416*, 811.

(8) Lekkerkerker, H. N. W.; Tuinier, R., *Colloids and the Depletion Interaction*. Springer, Dordrecht: 2011; Vol. 833.